



Responsivity and photo-transient response of Tb/Al/p-Si heterostructure solar detectors

A. E. H. Gaballah¹ · Abdallah Karmalawi¹

Received: 30 August 2023 / Accepted: 23 October 2023 / Published online: 24 November 2023
© The Author(s), under exclusive license to The Optical Society of India 2023

Abstract This work aims to investigate the design, fabrication, and characterization of a novel photodetector for light-sensing applications. The photodetector is based on Tb/Al/Cr/p-Si heterostructure and was integrated using the E-beam evaporation fabrication technique. The performance of the photodetector was evaluated through various experiments, including I–V characteristics, responsivity, and photo-transient time analysis. The I–V characteristics were measured under dark and different irradiance levels. The experimental results showed that the structure has a good and fast response to the light confirming its photodiode behavior where the photocurrent increases with increasing illumination intensity due to the formation of electron–hole pairs. The electrical parameters were explained according to the thermionic emission (TE) theory. Moreover, Cheung and Nord’s methods were used to determine the diode electronic parameters such as ideality factor (n), barrier height (Φ_0), and series resistance (R_s). The photo-transient characteristics of the heterostructure diode carried out under irradiance of about 1000 W/m^2 have shown a fast response to light. The uncertainty budget for the I–V curves was estimated and tabulated.

Keywords Tb · Al · Cr · p-Si heterojunction diode · I–V characteristics · Photo-transient response · Solar detector · Irradiance

Introduction

Over the last few decades, significant efforts have been dedicated to the construction and development of photodetectors based on new materials [1–3]. This has been motivated by a wide range of applications including digital imaging, remote sensing, photovoltaics, optical communication systems, and medical diagnostics [4]. Several materials have been used for the fabrication of photodetectors; silicon comes as a promising material due to its superior characteristics such as high absorption to light, small bandgap, and longtime stability [5–8]. Despite the drawbacks in the integration of III–V semiconductors monolithically with Si substrates due to the crystal lattice mismatch [9–11], it is considered one of the appealing structures for the next-generation, optoelectronics, light emitting diode (LED), and photodetectors devices. Furthermore, nanomaterials have opened the door for the development of optoelectronics devices due to their excellent chemical structure that allows the tunability of bandgap in addition to the high electrical conductivity they show [12–14]. Heterostructure materials have attracted much interest as efficient photodetectors by employing new material combinations as organic–inorganic structures [15–17].

Metal semiconductor photodiodes are particularly useful in the ultraviolet, visible, and IR light regions [18], Aluminum is a good candidate material widely used for this purpose [19, 20]. Its optical, electrical, and spectral response properties have been investigated by several research groups [21, 22] however the formation of aluminum oxide (Al_2O_3) due to the reaction with air limits its use since it strongly affects the optical performance of the resulting film [23]. Then, to overcome these limitations, a protective capping layer is usually added on the top to avoid oxidation without affecting its physical properties [24]. For that purpose, we used a thin layer of Terbium on top of the Aluminum

✉ A. E. H. Gaballah
ahmed.gaballah@nis.sci.eg

¹ Photometry and Radiometry Division, National Institute of Standards (NIS), Tersa St, Al-Haram, Giza 12211, Egypt

surface, despite several semiconducting materials, Terbium (Tb) possesses remarkable properties that can provide high-performance and cost-effective photodetectors due to its narrower bandgap and mechanical stability based on its atomic structure [25, 26]. Recently, Tb has received considerable attention in the manufacturing of optoelectronic devices because of not only its versatile characteristics but also its fabrication compatibility with nanostructures through different techniques [27, 28]. It has also been reported that doping nanomaterials with rare earth elements can yield enhanced photoluminescence (PL) properties [29–32].

To date, several deposition methods have been used for Tb [33–35]. To our knowledge, deposition by electron beam technique has not been deeply investigated. Furthermore, many fundamental properties of this semiconductor, such as the electrical, dielectric, and surface reactivity, remain poorly explored. This study provides valuable insights into the design and optimization of photodetectors for efficient light detection where a multilayer heterostructure photodiode based on a Terbium (Tb) thin film on top of an Aluminum (Al) layer was deposited on a Si substrate using the electron beam (e-beam) evaporation technique. A chromium layer (Cr) was deposited on the Si surface for more adhesive of the Al layer. Both the electrical and photo-response properties of the Tb/Al/Cr/p-Si photodiode were investigated under dark and different irradiance levels between (200–1080 W/m²) using the forward and reverse bias I–V measurements at room temperature. The photo-transient characteristic performed under irradiance of about 1000 W/m² and a biased voltage of 1.5 Volt showed that the prepared Tb/Al/Cr/p-Si heterostructure has a good and fast response to illumination. Additionally, the experimental design for I–V characteristics and photo response time systems was presented. Further, the uncertainty budget related to the I–V curves was estimated in detail.

Device fabrication and characterization

Tb/Al/Cr/p-Si heterostructure was fabricated with the deposition of Tb/Al thin films using an electron beam evaporation technique on a p-type Si wafer [36]. The Si substrate of orientation (100) was used as purchased without any further purification. Firstly, an interface layer of Cr of 3 nm thick was deposited on the Si substrate to increase the adhesion of Al layer with Si, then a thick layer of Al with a thickness of 20 nm was deposited on Cr layer, and finally, a protective capping layer of Tb with 6 nm thickness was deposited on top of Al surface as illustrated in Fig. 1. The film thickness was monitored during the deposition with a calibrated quartz-crystal monitor against a KLA-Tencor P-16 + Profilometer.

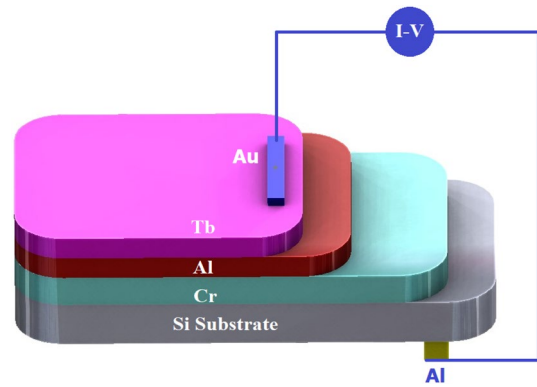


Fig. 1 Schematic diagram of fabricated Au/ Tb/Al/Cr/p-Si heterostructure photodetector device

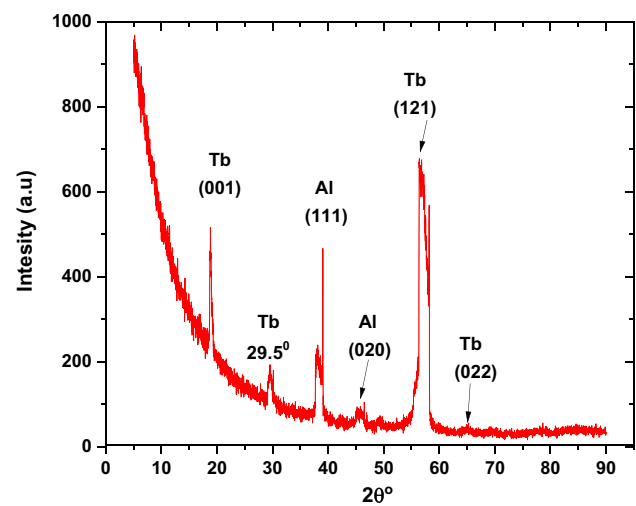


Fig. 2 XRD peaks of Tb/Al/Cr/p-Si heterostructure solar detector

The deposition chamber was pumped using a high vacuum Varian turbomolecular pump in series with a scroll pump. Small pieces of Tb and Al materials of 3–6 mm size with a purity of 99.9% were used as evaporated materials. The deposition rate for Al was kept at a constant rate of ~ 1.0 nm s⁻¹ while the deposition rate for Tb was ~ 0.5 nm s⁻¹ and the base pressure in the chamber was 10^{-6} Pa. The evaporation source was kept 40 cm away from the substrate, and the substrate holder was rotated during the deposition process for better film homogeneity and uniformity.

Figure 2 shows the X-ray diffraction pattern for the Tb/Al/Cr/p-Si heterostructure exhibiting distinct peaks indicating the crystallinity nature of the structure. The intensities show crystallographic planes similar to Al thin film with peaks appearing at 39° and 45° which correspond to the (1 1 1) and (0 2 0) planes. The Tb layer exhibits prominent peaks at 29.5° , 56.3° , and 65.6° which correspond to the (0 1 1), (1 2 1), and (0 2 2) planes [35, 37].

Experimental results

Current–voltage characterization

The I–V characteristics were measured at room temperature using a stabilized DC load power supply and two calibrated high-accuracy digital multimeter models Keithley 2010 where the voltage across the sample was measured simultaneously with the current through a reference shunt resistor. The sample's photocurrent and voltage characteristics were carried out under different irradiance levels using a Quartz Tungsten Halogen (QTH) lamp as a light source [38]. The I–V characteristics of the Tb/Al/Cr/p-Si heterostructure were measured under dark as well as different irradiance levels of 200, 500, 820 and 1050 W/m² which were measured using a calibrated radiometer traceable to a trap detector linked to the cryogenic radiometer. The incident light falls normally on a well-defined area of about 1 cm². The bias voltage was applied using a reference DC calibrator which swept the voltage from –2 Volte to +2 Volte with a sweep size of 1 mV. All devices are linked and controlled through a LabVIEW software which was developed by NIS as shown in Fig. 3.

The current–voltage characteristics of the Tb/Al/Cr/p-Si heterostructure photodiode were explained according to the thermionic emission theory under dark and different irradiance intensities [39]:

$$I = I_0 \left[\exp \frac{q(V - IR_s)}{nkT} \right] \quad (1)$$

where I_0 is the saturation current which is given by

$$I_0 = AA^*T^2 \left[\exp \frac{-q\phi_b}{kT} \right] \quad (2)$$

and n is the ideality factor, q is the electron charge, V is bias voltage, R_s is the series resistance, k is the Boltzmann constant, T is the temperature in Kelvin, A is the diode area, and A^* is Richardson constant ($A^* = 32 \text{ Acm}^{-2} \text{ K}^{-2}$ for p-type Si), ϕ_b is the barrier height [40, 41]. Figure 4. depicts the current–voltage (I–V) of Tb/Al/Cr/p-Si heterostructure photodiode at different irradiance levels and inset semi-logarithmic curve where I_0 and n were determined from the intercept and slope of the straight plot between $\ln(I)$ and V relationship of the voltage range from 0 to 0.4 V. The series resistance R_s represents the voltage drop across the diode and can be obtained throughout the relation [42]:

$$\left(\frac{dV}{d \ln I} \right) = \frac{nkT}{q} + IR_s \quad (3)$$

Additionally, Cheung proposed an alternative method to extract ideality factor (n), series resistance (R_s), and barrier height (ϕ_b) [43]. According to this method, $H(I)$ is defined as Cheung function and is given by

Fig. 3 Schematic diagram of the I–V and photo transient time response systems

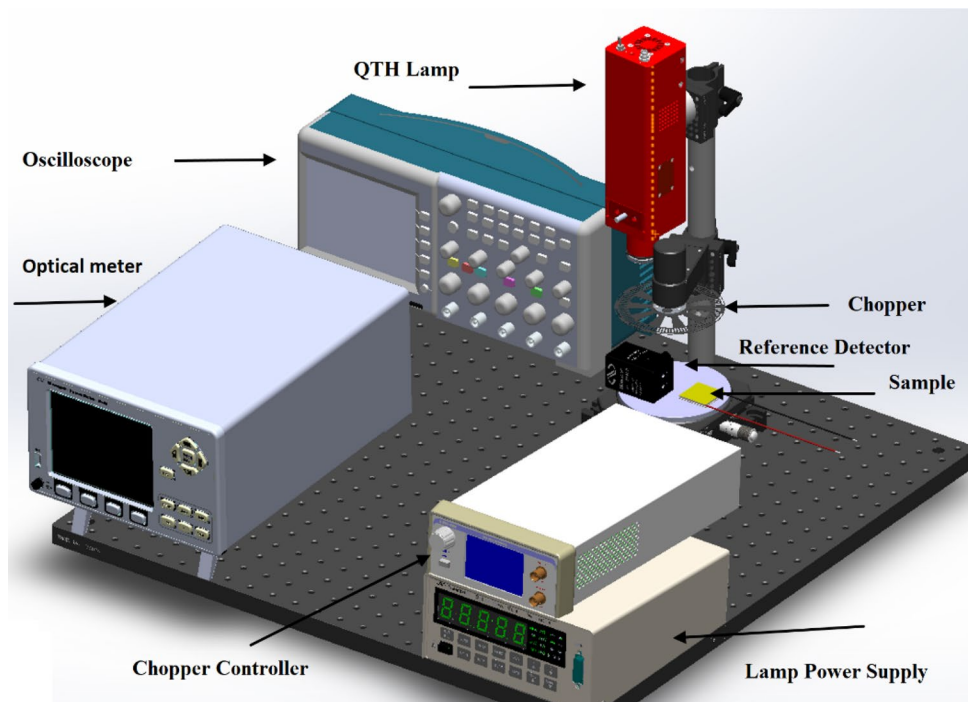
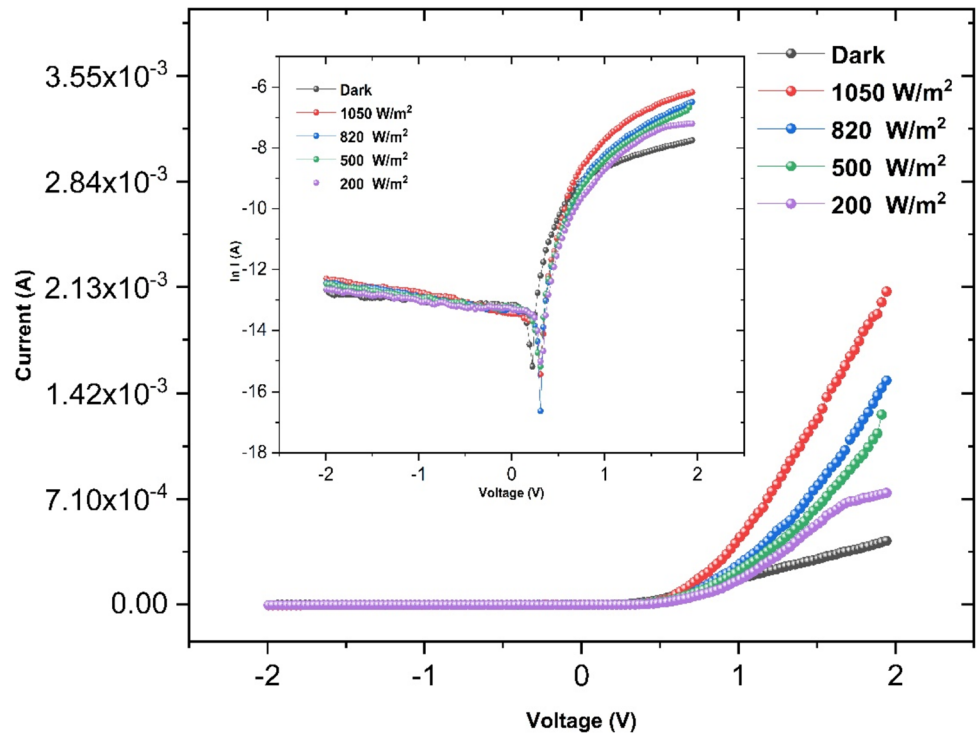


Fig. 4 Current–voltage (I–V) characteristic and inset semi-logarithmic curve of Tb/Al/Cr/p-Si heterostructure photodiode at different irradiance levels



$$H(I) = V - n \left(\frac{KT}{q} \right) \ln \left(\frac{I}{AA * T^2} \right) \tag{4}$$

where H(I) is given as

$$H(I) = n\phi_b + IR_s \tag{5}$$

Figure 5 displays $dV/d\ln(I)$ versus I for Tb/Al/Cr/p-Si heterostructure diode at a different level of irradiance. A plot of $dV/d\ln(I)$ versus current (I) will give R_s values as the slope and nkT/q as the intercept of the y-axis according to Eq. (3). The values of R_s and ideality factor (n) are listed in Table 1.

Figure 6 shows the plot of H (I) verse I give a straight line with an intercept equal to $n\phi_b$, while the slope gives the series resistance (R_s). The output parameters of the barrier height (Φ_0), and series resistance (R_s) are listed and tabulated in Table 1.

Norde proposed an alternative method to compare the barrier height and series resistance (R_s) of the Tb/Al/Cr/p-Si heterostructure [44]. According to this method, the Nord function $F(V)$ is defined as:

$$F(V) = \frac{V}{\gamma} - \frac{1}{\beta} \ln \left(\frac{1}{AA * T^2} \right) \tag{6}$$

where $\beta = q/KT$ and γ is a factor \geq the ideality factor (n), the active barrier height is given by

$$\phi_b = F(V_{min}) + \frac{V_{min}}{\gamma} - \frac{1}{\beta} \tag{7}$$

where $F(V_{min})$ is the minimum value of $F(V)$ corresponding to V_{min} .

$$R_s = \frac{\gamma - n}{\beta I_{min}} \tag{8}$$

where (I_{min}) is the current value corresponding to the minimum voltage value (V_{min}). Figure 7 shows the Norde function $F(V)$ against voltage for the Tb/Al/Cr/p-Si heterostructure photodiode at a different level of illumination. Table 1 provides the results of the ideality factor (n), barrier height (Φ_0), and series resistance (R_s) in accordance with Cheung, Nord, and conventional procedures. The Levenberg–Marquardt algorithm is used for linear fitting of Eqs. (1–9), and it compares the goodness of fit parameter, chi-square χ^2 , with confidence intervals. The fitting of the structure Tb/Al/Cr/p-Si was carried out in the voltage range of 0 to 0.5 V, which is the range where Ohm’s law is applicable. The slope and intercept of each curve were found in confidence intervals that have a high degree of confidence above 90%.

The observed variation in the ideality factor (n) can be attributed to the effects of series resistance, which causes a voltage drop across the interfacial thin film and the charge of the interface states with the bias in the low voltage

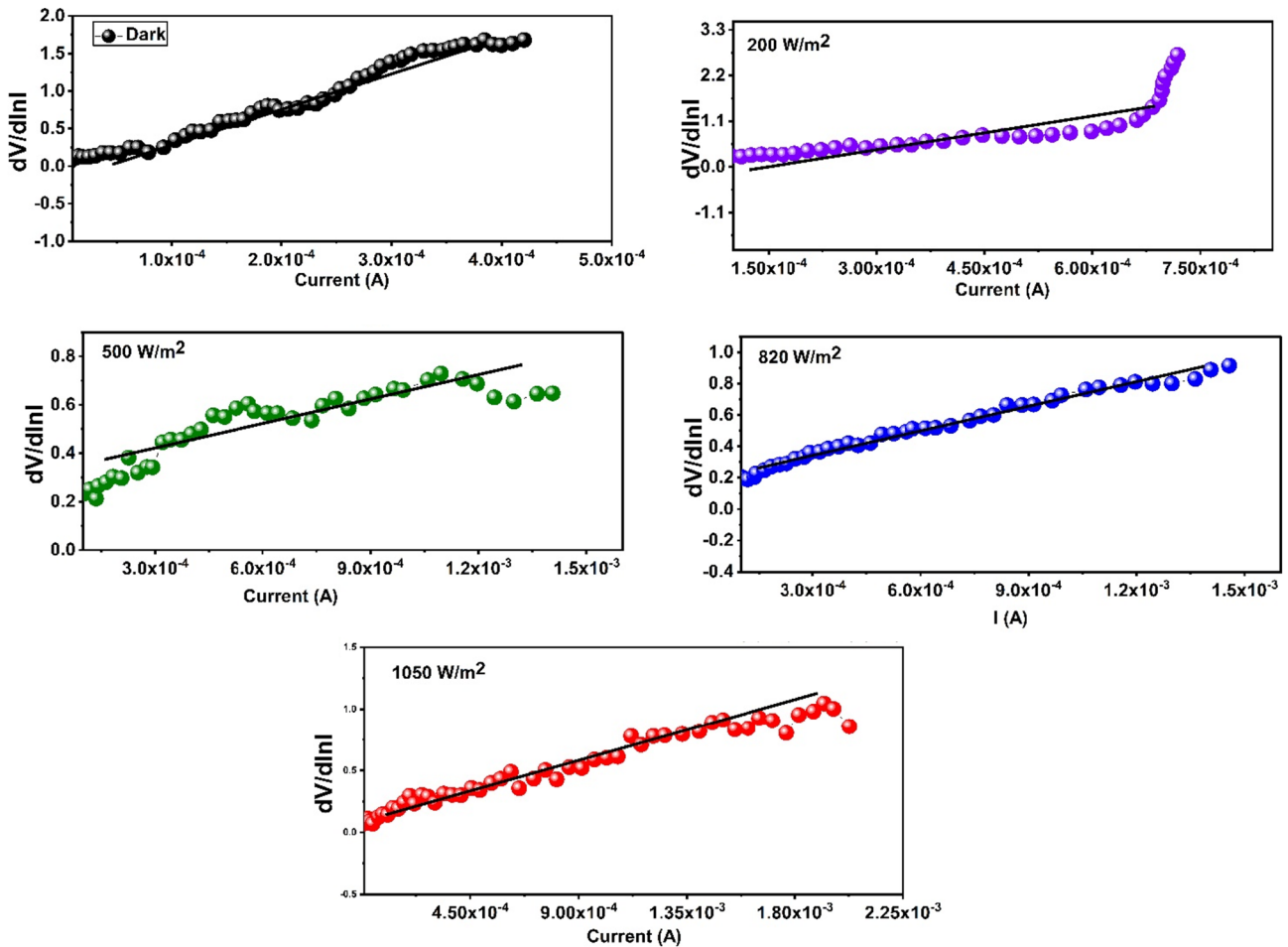


Fig. 5 $dV/d\ln I$ vs I of Tb/Al/Cr/p-Si heterostructure photodiode at different irradiance levels

Table 1 The calculated ideality factor, barrier height, and series resistance of Tb/Al/Cr/p-Si at different irradiance values were obtained from the various methods

Irradiance (W/m ²)	(TE)			Cheung (H)			$dV/d\ln I$		Nord (F)		
	n	ϕ_b eV	$R_s \Omega$	n	ϕ_b eV	$R_s \Omega$	n	$R_s \Omega$	n	ϕ_b eV	$R_s \Omega$
Dark	2.18	0.57	4.5×10^3	2.28	0.54	3.36×10^3	2.28	3.76×10^4	2.18	0.59	1.54×10^4
200	2.62	0.61	2.48×10^3	2.86	0.62	1.72×10^3	2.86	1.31×10^3	2.62	0.67	4.56×10^4
500	2.58	0.60	1.51×10^3	2.37	0.67	9.9×10^2	2.36	8.89×10^2	2.58	0.64	4.22×10^3
820	2.89	0.58	1.31×10^3	2.84	0.62	7.64×10^2	2.84	1.11×10^3	2.89	0.62	5.0×10^3
1050	1.71	0.68	9.24×10^2	3.73	0.54	4.8×10^2	3.73	5.12×10^2	1.67	0.64	2.35×10^5

region of the I–V diagram. Both the R_s and R_{sh} values have considerable influence on many electronic devices. The experimental R_s and R_{sh} values are determined by plotting structure resistance (R_i) vs. applied bias voltage (V) as shown in Fig. 9. In the forward biased region, R_s designates a nearly constant value of order $10^5 \Omega$ for voltage over 0.5 V. Subsequently, at negative bias voltage, the value of R_i decreases with increasing the voltage at different irradiance which corresponds to R_{sh} with a maximum

value of order $10^3 \Omega$ for. The lower value of series resistance R_s can be attributed to the transportation of charge carriers through the Cr diffusion layer or enhanced tunneling current through the barrier high using heavy doped n-type Si. The series resistance (R_s) and shunt resistance (R_{sh}) of Tb/Al/Cr/p-Si photodiode at different illumination intensities are seen in Fig. 8. The R_s designates a nearly constant value for positive voltages greater than 0.5 V while R_{sh} has nearly small values for negative voltages.

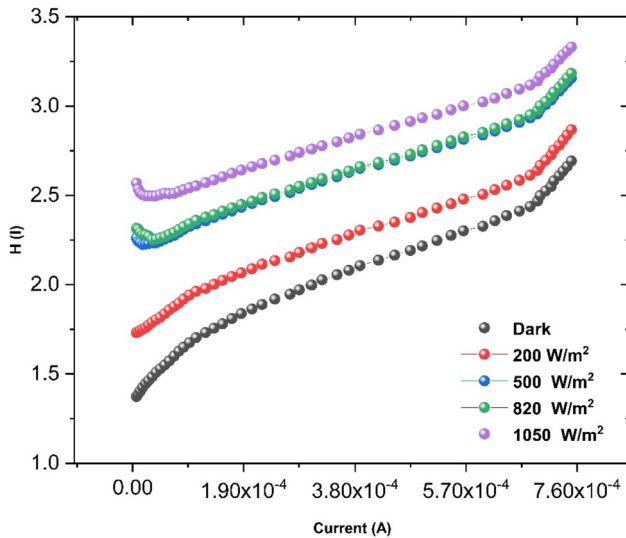


Fig. 6 H (I) vs I of Tb/Al/Cr/p-Si heterostructure photodiode at different irradiance levels

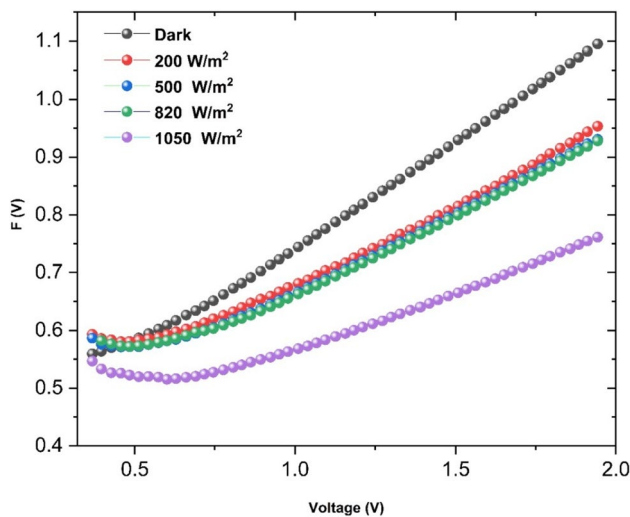


Fig. 7 F (V) vs Voltage of Tb/Al/Cr/p-Si heterostructure photodiode at different irradiance levels

The uncertainty budget for I–V measurements of Tb/Al/Cr/p-Si photodiode was calculated as the square root of the quadrature summation of each source of uncertainty inputs such as reference radiometer, solar simulator, the uncertainty of DC voltage-current measurements and uncertainty due to environmental conditions. Table 2 shows the uncertainty budget for I–V measurements and the related relative standard uncertainty for each input.

Uncertainty analysis plays a fundamental role in our research methodology and results. It serves to quantify and account for the potential errors and variations in the measurements, ensuring that our results are not only precise but

also reliable. By addressing the sources of uncertainty items and their associated values, we provide a more comprehensive view of the reliability of our measurements. Understanding uncertainties also aids in the proper interpretation of our findings and their potential implications, for more detailed information on this topic [45, 46]. For that purpose, the uncertainty budget includes the results of the measurement chains for irradiance, voltage, current, and temperature measurements that were reported according to GUM [47]. We considered the performance of the light source and the spectrum mismatch, furthermore, we also evaluated the standard uncertainty of voltage and current measurements using two calibrated digital Keithley multimeters, one of which was responsible for measuring drop voltage through a reference resistor. Table 2 lists the expanded uncertainty, which is normally provided at a confidence level of 95% for the coverage factor $k = 2$.

Photo-transient response measurement

The photo-transient response system is shown in Fig. 3. It consists of two high-speed silicon optical detectors as a reference detector for response time measurement model numbers 818-BB-21 and 818-BB-31 working in spectral ranges of 300 to 1100 nm and from 1000 nm up to 1600 nm respectively. The 818-BB-21 biased silicon detector has an active diameter of 0.40 mm with a rising time response of < 300 ps, and the 0.10 mm active diameter InGaAs detector with a < 175 ps rising time. A quartz tungsten halogen (QTH) lamp was used as a light source powered by a stabilized DC power supply of Newport, the beam emitted from the lamp passes through a controlled chopper equipped with a feedback frequency system. Both the sample under test and the reference detector are connected to two channels of digital storage 200MHz oscilloscope GDS-2202 [38]. The photo-transient response was performed via several on–off cycles under a QTH irradiation source at a biased voltage of 1.5 Volt [48, 49]. Figure 9 shows the photo-transient response of the Tb/Al/Cr/p-Si heterostructure photodiode; it is obvious that the structure displays good reproducibility and stability under several on–off chopped cycles of intermittent irradiation [50].

The photosensitivity (S_{ph}), is defined as the ratio of photocurrent (I_{ph}) to dark current (I_{dark}) thus it is calculated as follows:

$$S_{ph} = \frac{I_{ph}}{I_{dark}} \tag{9}$$

Figure 10 shows the photosensitivity (S_{ph}) plot versus illumination intensity power at different biased voltages. The heterostructure exhibits high photosensitivity as the photosensitivity increases with illumination intensity.

Fig. 8 Series resistance and in series shunt resistance of Tb/Al/Cr/p-Si photodiode at different illumination intensities

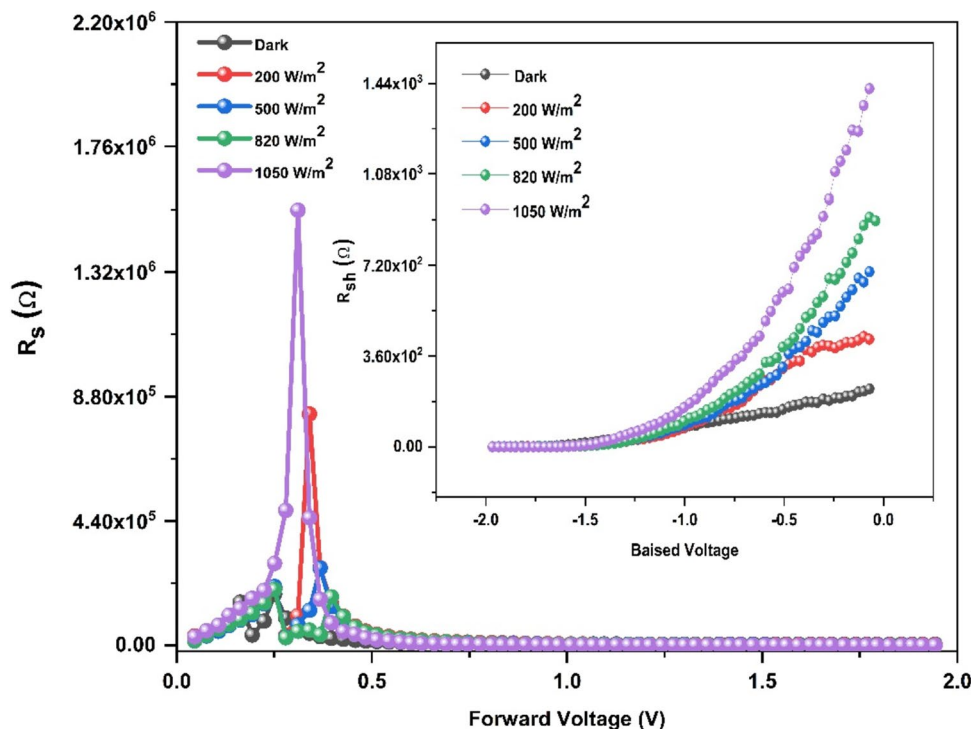


Table 2 The uncertainty budget of I–V characteristics for Tb/Al/Cr/p-Si photodiode

Uncertainty component	Relative standard uncertainty in %
1. Reference radiometer	1.00
Irradiance measurements (certificate)	1.00
irradiance repeatability	0.003
Non-linearity of the radiometer	0.0005
Reference radiometer (multimeter)	0.006
Reference radiometer drift	0.002
2. Solar simulator	0.53
Spatial non-uniformity	0.19
Spectral Mismatch	0.5
Dark background	0.01
Irradiance temporal stability	0.01
3. Uncertainty of DC voltage measurement	0.0050
DC voltage Signal repeatability	0.0050
Voltage DAQ (certificate)	0.00002
4. Uncertainty of DC measurement	0.001
5. Uncertainty of temperature measurement	0.2
Combined relative standard uncertainty in %	1.15
Expanded uncertainty ($k=2$) %	2.30

Conclusion

The I–V characteristics and photoresponsivity properties of the Tb/Al/Cr/p-Si heterostructure photodiode were

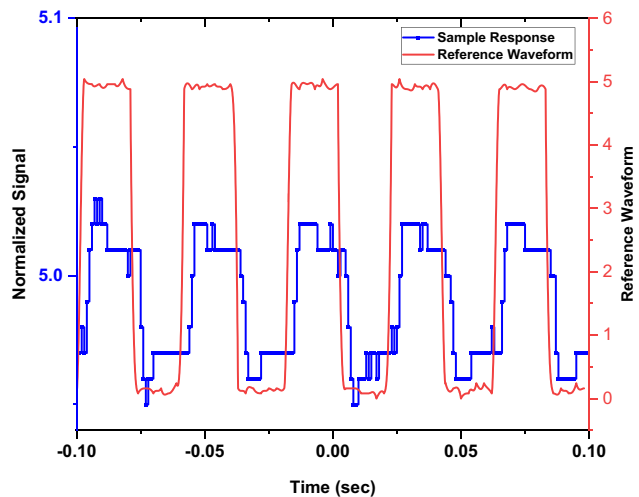


Fig. 9 Transient response of Tb/Al/Cr/p-Si heterostructure photodiode

measured in dark and under different illumination intensities in the range of 200–1000 W/m² using the I–V system. The standard thermionic emission (TE) theory was used to determine the electrical parameters of the heterostructure such as ideality factor (n), barrier height (Φ_0), and series resistance (R_s). Moreover, a comparative study has been done using an alternative method suggested by Cheung and Nord. The (Φ_0) and series resistance (R_s) obtained from both methods are in good agreement with the values obtained from the standard (TE) theory. The responsivity of the structure to illumination

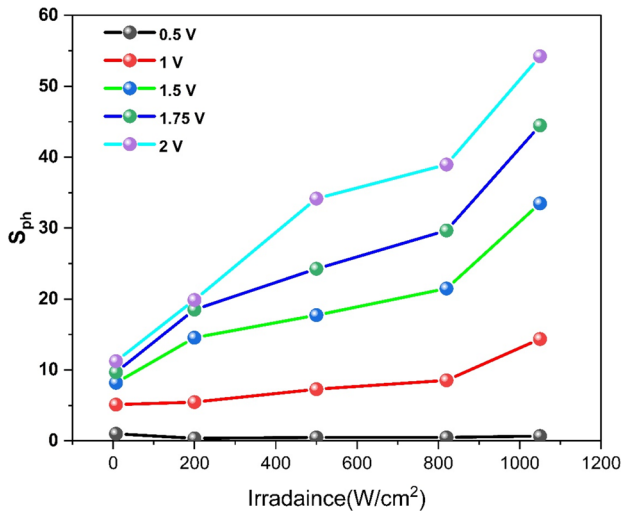


Fig. 10 The photosensitivity versus irradiance as a function of different biased voltages

indicates that photodiodes have the potential to be used as solar detectors, especially, in the forward region, where the photocurrent increases with increasing illumination intensity due to the formation of electron–hole pairs. The expanded uncertainty related to the I–V curves was estimated as 2.3% at a confidence level of $k = 2$.

Acknowledgements We would like to extend our sincere appreciation to The Science, Technology & Innovation Funding Authority (STDF) in cooperation with the Egyptian Knowledge Bank (EKB) for their funding for open access.

Declarations

Conflict of interest The authors declare no competing interests.

References

- B. Sekertekin, K. Ozel, A. Atilgan, A. Yildiz, Ultraviolet photodiode fabricated from TiO₂ nanorods/p-silicon heterojunction. *Mater. Lett.* **323**, 132565 (2022)
- A.B. Ullusan, A. Tataroglu, Ş Altundal, Y. Azizian-Kalanderagh, Photoresponse characteristics of Au/(CoFe₂O₄-PVP)/n-Si/Au (MPS) diode. *J. Mater. Sci. Mater. Electron.* **32**(12), 15732–15739 (2021)
- A. Ashery, A.E.H. Gaballah, G.M. Turkey, Current transport, photosensitive, and dielectric properties of PVA/n-Si heterojunction photodiode. *SILICON* (2021). <https://doi.org/10.1007/s12633-021-01260-8>
- A. Ashery, G. Said, W.A. Arafa, A.E.H. Gaballah, A.A.M. Farag, Structural and optical characteristics of PEDOT/n-Si heterojunction diode. *Synth. Met.* **214**, 92–99 (2016)
- M. Uslenghi, D. Faccini, M. Fiorini, S. Incorvaia, G. Toso, L. Schettini, M. Carminati, E. Fabbrica, C. Fiorini, M.G. Pelizzo, A.J. Corso, Development of a novel photon counting detector for UV spectrographs. *Proc. SPIE* **12191**, 121912O (2022)
- A. Karabulut, A. Dere, O. Dayan, A.G. Al-Sehemi, Z. Serbetci, A.A. Al-Ghamdi, F. Yakuphanoglu, Silicon based photodetector with Ru(II) complexes organic interlayer. *Mater. Sci. Semicond. Process.* **91**, 422–430 (2018)
- H.J. Syu, S.C. Shiu, C.F. Lin, Silicon nanowire/organic hybrid solar cell with efficiency of 8.40%. *Sol. Energy Mater. Sol. Cells* **98**, 267–272 (2012)
- A. Buyukbas-Ullusan, A. Tataroglu, Electrical characterization of silicon nitride interlayer-based MIS diode. *J. Mater. Sci. Mater. Electron.* **31**(12), 9888–9893 (2020)
- N. Jain, M.K. Hudait, III–V Multijunction solar cell integration with silicon: present status, challenges and future outlook. *Energy Harvest. Syst.* (2014). <https://doi.org/10.1515/ehs-2014-0012>
- J. Justice, C. Bower, M. Meitl, M.B. Mooney, M.A. Gubbins, B. Corbett, Wafer-scale integration of group III–V lasers on silicon using transfer printing of epitaxial layers. *Nat. Photon.* **6**(9), 610–614 (2012)
- M. Paladugu, C. Merckling, R. Loo, O. Richard, H. Bender, J. Dekoster, W. Vandervorst, M. Caymax, M. Heyns, Site selective integration of III–V materials on Si for nanoscale logic and photonic devices. *Cryst. Growth* **12**(10), 4696–4702 (2012)
- Z. Li, K. Xu, F. Wei, Recent progress in photodetectors based on low-dimensional nanomaterials. *Nanotechnol. Rev.* **7**(5), 393–411 (2018)
- W. Tian, H. Sun, L. Chen, P. Wangyang, X. Chen, J. Xiong, L. Li, Low-dimensional nanomaterial/Si heterostructure-based photodetectors. *InfoMat* **1**(2), 140–163 (2019)
- M.-S. Choi, T. Park, W.-J. Kim, J. Hur, High-Performance ultraviolet photodetector based on a zinc oxide nanoparticle and single-walled carbon nanotube heterojunction hybrid film. *Nanomaterials* (2020). <https://doi.org/10.3390/nano10020395>
- Z. Yang, Z. Fang, J. Sheng, Z. Ling, Z. Liu, J. Zhu, P. Gao, J. Ye, Optoelectronic evaluation and loss analysis of PEDOT:PSS/Si hybrid heterojunction solar cells. *Nanoscale Res. Lett.* **12**(1), 26 (2017)
- A. Ashery, S. Gad, H. Shaban, A.E.H. Gaballah, Heterostructure device based on graphene Oxide/TiO₂/n-Si for optoelectronic applications. *ECS J. Solid State Sci. Technol.* (2021). <https://doi.org/10.1149/2162-8777/abe1d9>
- N.M.A. Hadia, S. Eid, M. Shaban, S.H. Mohamed, A.M. Elsayed, A.M. Ahmed, M. Alzaid, A.A.A. Abdelazeez, W. El Malti, M. Rabia, Poly-3-Methyl Aniline-assisted spherical PbS quantum dots through the ionic adsorption deposition method as a novel and highly efficient photodetector in UV, Vis, and NIR regions. *Adsorpt. Sci. Technol.* **2022**, 1–12 (2022)
- P. Phukan, P.P. Sahu, High performance UV photodetector based on metal-semiconductor-metal structure using TiO₂-rGO composite. *Opt. Mater. (Amst)*. **109**, 110330 (2020)
- A. Fuad, D. Rusdiana, H. Saragih, T. Saragi, and M. Barmawi, Spectral Response of Al/Si Photodiode as IR Sensor, arXiv Prepr. cond-mat/0107213 (2001).
- A. Dubey, R. Mishra, Y. Hsieh, C. Cheng, B. Wu, L. Chen, S. Gwo, T. Yen, Aluminum plasmonics enriched ultraviolet GaN photodetector with ultrahigh responsivity, detectivity, and broad bandwidth. *Adv. Sci.* **7**(24), 2002274 (2020)
- K. Chongsri, W. Pecharapa, UV Photodetector based on Al-doped ZnO nanocrystalline sol-gel derived thin films. *Energy Procedia* **56**, 554–559 (2014)
- Y. Zhao, W.R. Donaldson, Ultrafast UV AlGaN metal–semiconductor–metal photodetector with a response time below 25 ps. *IEEE J. Quantum Electron.* **56**(3), 1–7 (2020)
- A.E.H. Gaballah, P. Nicolosi, N. Ahmed, K. Jimenez, G. Pettinari, A. Gerardino, P. Zuppella, Vacuum ultraviolet quarter wave plates based on SnTe/Al bilayer: Design, fabrication, optical and ellipsometric characterization. *Appl. Surf. Sci.* **463**, 75–81 (2018)

24. J. Hennessy, K. Balasubramanian, C.S. Moore, A.D. Jewell, S. Nikzad, K. France, M. Quijada, J. Astron. Performance and prospects of far ultraviolet aluminum mirrors protected by atomic layer deposition. *J. Astron. Telesc. Instrum. Syst.* **2**(4), 041206 (2016)
25. R. Malmhäll, Extraordinary Hall resistivity in amorphous terbium–iron thin films and its temperature dependence. *J. Appl. Phys.* **54**(9), 5128–5131 (1983)
26. A.S. Kalyakina, V.V. Utochnikova, E.Y. Sokolova, A.A. Vashchenko, L.S. Lepnev, R. Van Deun, A.L. Trigub, Y.V. Zubavichus, M. Hoffmann, S. Mühl, N.P. Kuzmina, OLED thin film fabrication from poorly soluble terbium o-phenoxybenzoate through soluble mixed-ligand complexes. *Org. Electron.* **28**, 319–329 (2016)
27. I.L.P. Raj, S. Valanarasu, S. Vinoth, N. Chidhambaram, R.S.R. Isaac, M. Ubaidullah, S.F. Shaikh, B. Pandit, Highly sensitive ultraviolet photodetectors fabricated from rare earth metal ions doped NiO thin films via nebulizer spray pyrolysis method. *Sens. Actuators A Phys.* **333**, 113242 (2022)
28. M.D. Devi, A.V. Juliet, K. Hariprasad, V. Ganesh, H.E. Ali, H. Algarni, I.S. Yahia, Improved UV Photodetection of Terbium-doped NiO thin films prepared by cost-effective nebulizer spray technique. *Mater. Sci. Semicond. Process.* **127**, 105673 (2021)
29. L. Zhang, C.L. Heng, C.N. Zhao, W.Y. Su, Y.K. Gao, P.G. Yin, T.G. Finstad, On the structure and ultraviolet emission of terbium doped zinc oxide thin films on silicon after high temperature treatment. *Res. Phys.* **32**, 105121 (2022)
30. A.V. Paduraru, O. Oprea, A.M. Musuc, B.S. Vasile, F. Iordache, E. Andronescu, Influence of Terbium ions and their concentration on the photoluminescence properties of hydroxyapatite for biomedical applications. *Nanomaterials* (2021). <https://doi.org/10.3390/nano11092442>
31. M.I. Kozlov, A.N. Aslandukov, A.A. Vashchenko, A.V. Medved'ko, A.E. Aleksandrov, E.V. Latipov, A.S. Goloveshkin, D.A. Lypenko, A.R. Tameev, V.V. Utochnikova, Toward efficient terbium-based solution-processed OLEDs: Hole mobility increase by the ligand design. *J. Alloys Compd.* **887**, 161319 (2021)
32. S. Carmona-Téllez, C. Falcony, M. Aguilar-Frutis, G. Alarcón-Flores, M. García-Hipólito, R. Martínez-Martínez, Photoluminescence, conductivity and structural study of terbium doped ZnO films grown on different substrates. *Mater. Sci. Semicond. Process.* **94**, 51–56 (2019)
33. Z. Wang, H. Liu, S. Wang, Z. Rao, Y. Yang, A luminescent Terbium-Succinate MOF thin film fabricated by electrodeposition for sensing of Cu²⁺ in aqueous environment. *Sens. Actuators B Chem.* **220**, 779–787 (2015)
34. E. Pereyra-Perea, M.R. Estrada-Yañez, M. García, Preliminary studies on luminescent terbium-doped thin films prepared by the sol-gel process. *J. Phys. D Appl. Phys.* **31**(3), L7 (1998)
35. S.V. Belaya, V.V. Bakovets, A.I. Boronin, S.V. Koshcheev, M.N. Lobzareva, I.V. Korolkov, P.A. Stabnikov, Terbium oxide films grown by chemical vapor deposition from terbium(III) dipivaloyl-methanate. *Inorg. Mater.* **50**(4), 379–386 (2014)
36. A. E. H. Gaballah, P. Zuppella, N. Ahmed, K. Jimenez, G. Pettinari, A. Gerardino, and P. Nicolosi, “A table top polarimetric facility for the EUV spectral range: implementations and characterization,” in *Proc. SPIE* **10235**, p. 102350X, *Proc. SPIE* (2017).
37. S. Carmona-Téllez, C. Falcony, M. Aguilar-Frutis, G. Alarcón-Flores, M. García-Hipólito, R. Martínez-Martínez, White light emitting transparent double layer stack of Al₂O₃:Eu³⁺, Tb³⁺, and Ce³⁺ films deposited by spray pyrolysis. *ECS J. Solid State Sci. Technol.* (2013). <https://doi.org/10.1149/2.017306jss>
38. A.M. Karmalawi, A.A. Abdelmageed, Development of a detector-based absolute spectral power responsivity scale in the spectral range of 300–1600 nm. *J. Mater. Sci. Mater. Electron.* **32**(4), 5215–5221 (2021)
39. S. Demirezen, A.G. Al-Sehemi, A. Yüzer, M. Ince, A. Dere, A.A. Al-Ghamdi, F. Yakuphanoglu, Electrical characteristics and photosensing properties of Al/symmetrical CuPc/p-Si photodiodes. *J. Mater. Sci. Mater. Electron.* **33**(26), 21011–21021 (2022)
40. S.M. Sze, K.K. Ng, *Physics of Semiconductor Devices* (John Wiley & Sons Inc, Hoboken, NJ, USA, 2006)
41. E. H. Rhoderick and R. H. Williams, *Metal-semiconductor contacts*, Clarendon Press ; Oxford University Press, Oxford [England]; New York (1988).
42. A. Tataroglu, R. Ocaya, A. Dere, O. Dayan, Z. Serbetci, A.G. Al-Sehemi, M. Soylu, A.A. Al-Ghamdi, F. Yakuphanoglu, Ruthenium(II) complex based photodiode for organic electronic applications. *J. Electron. Mater.* **47**(1), 828–833 (2018)
43. S.K. Cheung, N.W. Cheung, Extraction of Schottky diode parameters from forward current-voltage characteristics. *Appl. Phys. Lett.* **49**(2), 85–87 (1986)
44. H. Norde, A modified forward I-V plot for Schottky diodes with high series resistance. *J. Appl. Phys.* **50**(7), 5052–5053 (1979)
45. A.M. Karmalawi, D.A. Rayan, M.M. Rashad, Establishment and evaluation of photovoltaic quantum efficiency system at central metallurgical research and development institute. *Opt. Int. J. Light Electron Opt.* **217**, 164931 (2020)
46. A.M. Karmalawi, Characterization, traceability, and uncertainty estimation of reference solar panel module measurements using pulsed solar simulators and reference solar cells. *Acta IMEKO* **12**(3), 1–9 (2023)
47. J. H. Williams, Guide to the Expression of Uncertainty in Measurement (the GUM), in *Quantifying Measurement The tyranny of numbers*, IOP Publishing 6–9 (2016).
48. A. Verma, P. Chaudhary, R.K. Tripathi, B.C. Yadav, Transient photodetection studies on 2D ZnO nanostructures prepared by simple organic-solvent assisted route. *Sens. Actuators A Phys.* **321**, 112600 (2021)
49. B. Stannowski, H. Stiebig, D. Knipp, H. Wagner, Transient photocurrent response of three-color detectors based on amorphous silicon. *J. Appl. Phys.* **85**(7), 3904–3911 (1999)
50. J.-Y. Kim, S.-A. Oh, K.M. Yu, B.S. Bae, E.-J. Yun, Transient photocurrent responses in amorphous Zn-Sn-O thin films. *J. Korean Phys. Soc.* **66**(7), 1039–1044 (2015)

Publisher's Note Springer Nature remains neutral with regard to jurisdictional claims in published maps and institutional affiliations.

Springer Nature or its licensor (e.g., a society or other partner) holds exclusive rights to this article under a publishing agreement with the author(s) or other rightsholder(s); author self-archiving of the accepted manuscript version of this article is solely governed by the terms of such publishing agreement and applicable law.